Functional Role of the Conserved Active Site Proline of Triosephosphate Isomerase[†,‡]

Marco G. Casteleijn,[§,∥] Markus Alahuhta,[§,⊥] Katrin Groebel,[∥] Ibrahim El-Sayed,[#] Koen Augustyns,[#] Anne-Marie Lambeir,[△] Peter Neubauer,[∥] and Rik K. Wierenga*[,⊥]

Biocenter Oulu and Department of Biochemistry and Department of Process and Environmental Engineering and Bioprocess Engineering Laboratory, University of Oulu, P.O. Box 3000, FIN-90014 Oulu, Finland, and Laboratory of Medicinal Chemistry and Laboratory of Medical Biochemistry, University of Antwerp, Wilrijk, Belgium

Received August 18, 2006; Revised Manuscript Received October 9, 2006

ABSTRACT: The importance of the fully conserved active site proline, Pro168, for the reaction mechanism of triosephosphate isomerase (TIM) has been investigated by studying the enzymatic and crystallographic properties of the P168A variant of trypanosomal TIM. In TIM, Pro168 follows the key catalytic residue Glu167, situated at the beginning of the flexible active site loop (loop 6). Turnover numbers of the P168A variant for its substrates are reduced approximately 50-fold, whereas the K_m values are approximately 2 times lower. The affinity of the P168A variant for the transition state analogue 2-phosphoglycolate (2PG) is reduced 5-fold. The crystal structures of unliganded and liganded (2PG) P168A show that the phosphate moiety of 2PG is bound similarly as in wild-type TIM, whereas the interactions of the carboxylic acid moiety with the side chain of the catalytic Glu167 differ. The unique properties of the proline side chain at position 168 are required to transmit ligand binding to the conformational change of Glu167: the side chain of Glu167 flips from the inactive swung-out to the active swung-in conformation on ligand binding in wild-type TIM, whereas in the mutant this conformational change does not occur. Further structural comparisons show that in the wild-type enzyme the concerted movement of loop 6 and loop 7 from unliganded-open to liganded-closed appears to be facilitated by the interactions of the phosphate moiety with loop 7. Apparently, the rotation of 90° of the Gly211-Gly212 peptide plane of loop 7 plays a key role in this concerted movement.

Active sites of enzymes are shaped to be complementary to the transition state of the catalyzed reaction in order to facilitate optimal catalysis (*1*, *2*). Strained conformations of residues near active sites occur in order to achieve proper geometry. Examples of strained main chain and side chain conformations have been described in the literature (*3*−*5*). Recently, another form of strain, the planar proline ring of Pro168, was discovered in the enzyme triosephosphate isomerase (TIM;[1] E.C. 5.3.1.1). This enzyme catalyzes the interconversion of DHAP and GAP (Figure 1) via a *cis*-enediolate intermediate (*6*, *7*). TIM is a dimeric enzyme consisting of two identical subunits, each having the classical

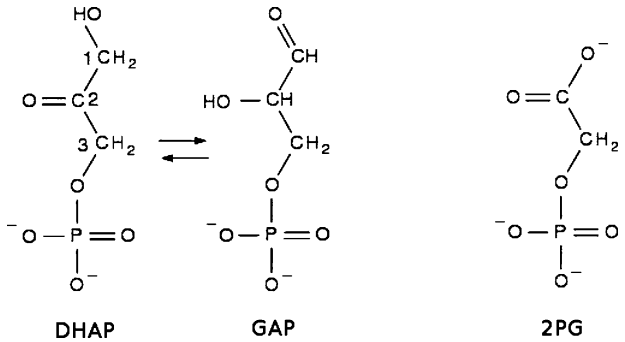

FIGURE 1: TIM catalyzes the interconversion of an α-hydroxy ketone (DHAP) and a chiral α-hydroxyaldehyde (GAP). The covalent structure of the transition state analogue 2-phosphoglycolate (2PG) is also shown.

$(\beta\alpha)_8$ TIM-barrel fold. The active site is shaped by the loops emerging from the eight parallel β-strands of the TIM barrel, referred to as loops 1−8. When bound to the enzyme, the substrate is sequestered by the active site and shielded from the bulk solvent because of the closure of one of the catalytic loops: loop 6. Classically, loop 6 concerns residues 168−178 (*8*), following immediately after the catalytic glutamate, Glu167. The closure of loop 6 is correlated with the movement of the side chain of Glu167 from the inactive swung-out to the active swung-in conformation (*9*−*11*).

The planar, strained proline conformation of Pro168 was noted in the atomic resolution structure of leishmanial TIM, in complex with the transition state analogue 2-phosphogly-

[†] This research has been supported by grants from the Academy of Finland (Project 53923).

[‡] The coordinates and structure factors of P168A have been deposited at the RCSB-PDB with entry codes 2j24 (unliganded) and 2j27 (liganded).

* To whom correspondence should be addressed. Telephone: +358-(8)5531199. Fax: +358(8)5531141. E-mail: rik.wierenga@oulu.fi.

[§] These authors contributed equally to this work.

[∥] Department of Process and Environmental Engineering and Bioprocess Engineering Laboratory, University of Oulu.

[⊥] Biocenter Oulu and Department of Biochemistry, University of Oulu.

[#] Laboratory of Medicinal Chemistry, University of Antwerp.

[△] Laboratory of Medical Biochemistry, University of Antwerp.

[1] Abbreviations: 2PG, 2-phosphoglycolate; BHAP, bromohydroxyacetone phosphate; GAP, D-glyceraldehyde 3-phosphate; DHAP, dihydroxyacetone phosphate; DTT, dithiothreitol; IPTG, isopropyl β-D-thiogalactopyranoside; TbTIM, trypanosomal triosephosphate isomerase; TIM, triosephosphate isomerase; T_m, melting temperature.

10.1021/bi061683j CCC: $33.50
Published on Web 12/19/2006

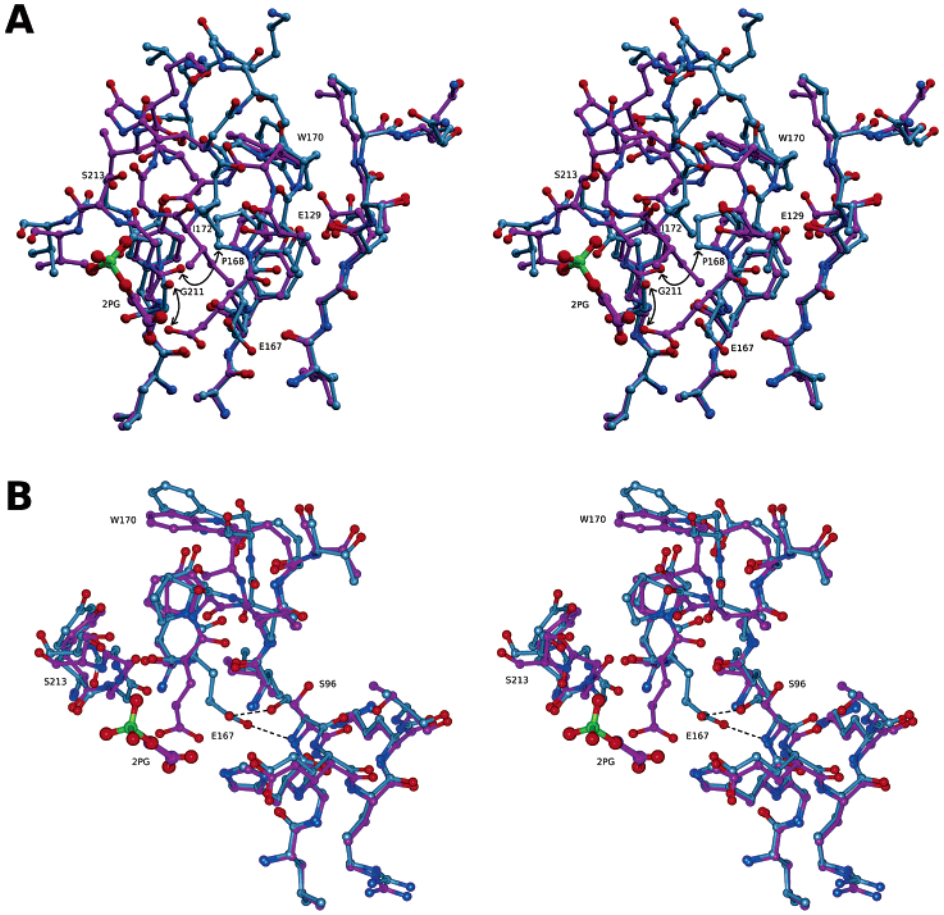

FIGURE 2: Structure comparison of the conformational switch from open (unliganded; cyan) to closed (liganded with 2PG; purple), as seen for wild-type TIM. (A) Pro168 is at the center of the view, and included in this diagram are residues of loop 5 (residues 127−132), loop 6 (residues 165−178), and loop 7 (residues 209−214). The curved arrows mark the clashes of O(Gly211) with atoms of Glu167 and Pro168, when comparing unliganded and liganded conformations. (B) Glu167 is at the center of the view, and included in this diagram are residues of loop 4 (residues 93−100), loop 5 (residues 127−130), loop 6 (residues 166−170), and loop 7 (residues 210−213). The dotted lines indicate the hydrogen-bonding interactions between Glu167 and Ser96 in the unliganded state.

colate (2PG) (*12*). Proline rings are normally puckered, with the CG atom being puckered either upward (χ_1 is approximately −30°) or downward (χ_1 is approximately +30°), whereas the planar ring conformation is rarely seen (*13*). The five-membered ring of the proline side chain provides this amino acid with several other unique properties (*14*, *15*), in particular its conformational rigidity and the absence of a proton on the α-amino group.

Pro168 is located at the beginning of the flexible loop 6 (Figure 2), immediately following after the catalytic glutamate, Glu167. In both the unliganded (open) and the liganded (closed) conformation of wild-type TIM the Glu167-Pro168 peptide is a *trans* peptide bond. This region of the structure is known to be well-defined in the electron density maps in both conformations. In the open, unliganded conformation of loop 6, Pro168 is puckered in the down conformation ($\chi_1 = +40^\circ$). A systematic structural analysis of the pyrrolidine puckering for proline residues with a preceding *trans* peptide bond (*13*) shows that this is a common conformation, seen in many protein structures. The strained planar conformation of Pro168 is observed in the liganded TIM structure but not in the unliganded conformation. It has been analyzed with QM/MM calculations, which showed that its planar conformation indeed has considerable strain. This strain (approximately 9 kJ/mol for a planar proline in vacuo) is compensated by van der Waals interactions with the side chains of the neighboring residues Tyr166 and Ala171 (*16*). It has been speculated that this strain could be important for loop opening and product release, once the reaction cycle has been completed (*12*, *16*). Sequence comparisons of more than 100 TIM sequences (*17*) show that Pro168 is a completely conserved residue, suggesting also that this proline must have an important functional role. Indeed, directed evolution experiments have confirmed that only a proline at this position is compatible with full activity (*18*).

In the unliganded-open form, loop 6 interacts with loop 5 (Figure 2). The interactions between loop 6 and loop 5 are not very tight as loop 6 characteristically has high *B*-factors in this open conformation (*19*). In the liganded-closed form, the tip of loop 6 moves away from loop 5 toward loop 7. Loop 7 refers to the YGGS peptide (residues 210−213) and loop 6 is hydrogen bonded to Tyr210 and Ser213 in the closed form (Figure 2). Several studies have addressed the dynamics of this loop motion, using for example NMR (*20*, *21*), temperature-jump relaxation spectroscopy (*22*), and computational approaches (*23*, *24*). The closure of loop 6 is actually a concerted movement in which both loop 6 and loop 7 change conformation (*17*). This is in agreement with the observation of an unliganded, but closed conformation of rabbit TIM, in which both loop 6 and loop 7 have adopted the closed conformation (*25*); similarly, a liganded, but open conformation has been observed for plasmodium TIM in

which both loop 6 and loop 7 have adopted the open conformation (*26*). The conformational switch of loop 6 is a rigid body movement of the tip of loop 6 (residues Ile172-Gly173-Thr174-Gly175) of approximately 7 Å, coupled to a relatively small change of the ϕ/ψ values of the N-terminal and C-terminal hinges (*8*, *27*). The importance of the sequence conservation patterns of these loop 6 hinge regions has been studied extensively (*17*, *28*, *29*).

The conformational switch of loop 7 (*30*) concerns a rotation of two peptide bonds: a rotation of 90° of the peptide plane after Gly211 and of 180° of the peptide plane after Gly212. The peptide flip of the Gly212-Ser213 peptide bond is required to provide a hydrogen-bonding partner for the phosphate moiety of the substrate (Figure 2). The rotation of 90° of the peptide plane after Gly211 is required to allow the movement of the side chain of the catalytic glutamate (Glu167) from the swung-out position to the swung-in position. O(Gly211) in its unliganded position is at 2.6 Å from the Glu167 side chain oxygen in its (liganded) swung-in position, but in the liganded structure the main chain oxygen of Gly211 is rotated away (Figure 2). In its new conformation O(Gly211) points toward the CD atom of the side chain of Pro168, pushing it away from its unliganded position (Figure 2). The distance between O(Gly211) (in the closed loop 7 position) and the CD(Pro168) atom (in its unliganded, open position) is 2.5 Å, and the geometry is not favorable for C−H···O hydrogen bonding (*31*, *32*). Consequently, in the closed structure Pro168 has moved away from O(Gly211), and this distance has become 3.3 Å.

The interconversion of DHAP and GAP by TIM concerns the transfer of protons (Figure 1). The precise mechanism of this proton transfer has been investigated intensively (*33*−*36*). The detailed studies on chicken TIM (*37*) and yeast TIM (*38*) have shown that the enzyme has evolved to catalyze this reaction in vivo at maximal efficiency, and the free energy barriers for ligand binding, conformational changes, and the chemical conversion step have become similar. The key catalytic residue involved in this proton shuttling is the catalytic glutamate: Glu167 (*7*). In its active, swung-in conformation this side chain points to the ligand and initiates the isomerase reaction by abstracting a proton from the C1 atom of the α-hydroxy ketone or from the C2 atom of the α-hydroxyaldehyde, respectively (Figure 1). In the conformational switch from the inactive swung-out to the active swung-in conformation the carboxyl group moves approximately 2.8 Å, and its two hydrogen-bonding interactions with the main chain and side chain of Ser96 are lost (Figure 2). The mechanism triggering this conformational change from swung-out to swung-in on ligand binding is poorly understood, but it has been suggested to be correlated with the small rearrangements of the Glu167-Pro168 region on loop 6 closure (*11*).

The proline side chain of Pro168 points away from the active site toward the interior of the protein and is surrounded by the side chains of the aromatic residues Tyr166, Trp170 (loop 6), and Tyr210 (loop 7), as well as Ala171 of loop 6 (Figure 2). In the liganded-closed form CB(Ala171) and the aromatic ring of Tyr166 favor the planar structure of the proline ring of Pro168 (*12*, *16*). In the open conformation the side chains of Trp170-Ala171 have moved away from the proline side chain, allowing it to adopt its unstrained down puckered conformation ($\chi_1 = 40°$) (Figure 2). In order to investigate which structural features of the Pro168 pyrrolidine side chain are important for its function, the kinetic and structural properties of the P168A variant were determined. Only a few other studies have investigated the importance of a proline for the proper active site geometry in other enzymes (*39*−*41*). In particular, the studies by Palfey et al. (*41*) suggest that the rigidity of the proline residue is important for transmitting a structural switch to the catalytic site of the enzyme *p*-hydroxybenzoate hydroxylase.

In the P168A studies reported here it is shown that mutating the proline into an alanine reduces the catalytic efficiency. The structural data show that the presence of the proline side chain is required for transmitting the signal of ligand binding and loop 6 closure to the Glu167 side chain. Only in the presence of a proline at position 168 does the Glu167 side chain adopt the catalytically competent swung-in conformation.

MATERIALS AND METHODS

Materials. Unless specifically mentioned, all commercial chemicals were used as obtained without further purification. Cation-exchange resin Dowex 50 was obtained from Aldrich. NADH, NAD, DL-glyceraldehyde 3-phosphate (diethylacetyl, monobarium salt), dithiothreitol (DTT), EDTA, dihydroxyactone phosphate, glyceraldehyde-3-phosphate dehydrogenase, α-glycerol-3-phosphate dehydrogenase, casein hydrolysate, and potassium dihydrogen arsenate were purchased from Sigma. 2PG was purchased from ProSyntest Ltd. (Estonia).

Bromohydroxyactetone phosphate (BHAP) was prepared as follows: bromoacetyl bromide (4.64 g, 23 mmol) in 25 mL of dry ether was added to ∼3 g of an alcohol-free ethereal solution of diazomethane (*42*) (∼200 mL, pale yellow color) at 0 °C (*Caution*! Diazomethane is highly explosive and carcinogenic). After 5 min, a few drops of glacial acetic acid were added dropwise with gentle stirring to destroy the excess of diazomethane. The solvent was removed under reduced pressure. The residue (yellow oil) was chromatographed on silica gel in ethyl acetate/hexane (1:5) to give 2.42 g (∼65%) of pure bromodiazoacetone (*43*) as a yellow oil [^{1}H NMR (400 MHz, $CDCl_3$): δ 3.84 (s, 2H, CH_2Br), 5.81 (br s, 1H, CHN_2) ppm. MS (ESI): m/z = 157 ($M^+ + Na - N_2$)]. Bromodiazoacetone (2.40 g, 14.73 mmol) in 15 mL of dry ether was added to phosphoric acid crystals (2.90 g, 29.60 mmol) in 100 mL of dry ether under nitrogen and cooled at 0 °C. A few drops of boron trifluoride etherate were added. The reaction mixture was kept at room temperature for 12 h under nitrogen gas. The progress of the reaction was monitored by thin-layer chromatography until the complete consumption of bromodiazoacetone was observed. The ether was removed under reduced pressure to yield BHAP (*44*) as viscous yellow oil [MS (ESI): m/z = 233 ($M^+ + 1$), 235 ($M^+ + 2$)].

Reaction buffers and media used were composed as follows. Buffer A: 100 mM triethanolamine hydrochloride (TEA), 1 mM EDTA, 1 mM DTT, 1 mM NaN_3, pH 7.6 (at 25 °C). Buffer B: 20 mM TEA, 1 mM EDTA, 1 mM DTT, 1 mM NaN_3, pH 8 (at 25 °C). Buffer C: 20 mM Tris-HCl, 100 mM NaCl, pH 7.0 (at 25 °C). M9ZB medium (per liter): 10 g of casein hydrolysate (Sigma), 5 g of NaCl, 0.5 g of NH_4Cl, 1.5 g of KH_2PO_4, 1.6 g of Na_2HPO_4, 2 g of D-glucose, and 0.5 mM $MgSO_4$.

DNA Methods. Site-directed mutagenesis was performed by PCR using a QuickChange site-directed mutagenesis kit (Stratagene). The expression plasmid pET3a (Novagen) containing wild-type trypanosomal TIM was used as a template. The mutagenic primers used were P168A sense (+), 5′-CGCCTACGAAGCCGTTTGGGCCATTGGTACCG-3′, and P168A compl (−), 5′-ACCAATGGCCCAAACG-GCTTCGTAGGCGATGAC-3′.

The complete DNA sequence of the TIM gene including the mutations was verified by using sequencing with the DYEnamic ET terminator cycle sequence kit (GE Healthcare). *Escherichia coli* TOP10 cells (Invitrogen) were used as the host strain for plasmid production. Plasmids were then transformed to *E. coli* strain BL21 pLysS (Invitrogen) for protein production.

Protein Expression and Purification. Expression of the trypanosomal TIM (TbTIM) and its P168A variant was carried out in *E. coli* BL21 pLysS. The transformants were grown in M9ZB medium with 100 μg mL^{-1} ampicillin and 35 μg mL^{-1} chloramphenicol at 37 °C and 180 rpm on a rotary shaker. Cells were induced at an OD_{600} of about 0.5 with 0.4−1 mM isopropyl β-D-thiogalactopyranoside (IPTG) and grown for another 8−14 h at 18 °C under continuous shaking. Cell pellets were stored at −20 °C. The cells were lysed by thawing at room temperature by the action of T7 lysozyme expressed on the plasmid pLysS. The cell extract was treated with DNase, RNase, and $MgCl_2$. The resulting extract was brought to 45% saturation on ice with ammonium sulfate for 15 min, and the precipitated proteins were removed by centrifugation (15 min at 17000*g*). The resulting supernatant was brought to 65% saturation on ice with ammonium sulfate for 15 min and centrifuged for 15 min at 17000*g* to yield a protein pellet. The protein pellet was resuspended in buffer B and dialyzed with a Spectra/POR membrane with a cutoff value of 12−14 kDa (Spectrum) o/n against buffer B. Dialysate was loaded to a CM-Sepharose column (GE Healthcare) calibrated with buffer B and eluted with a 5−200 mM NaCl gradient of 150 mL. The purity of all TIM variants was checked by SDS−PAGE using Coomassie staining. Eluate buffer was replaced by buffer C using a centrifugal concentrator with a 15 kDa NMWL membrane at 4000*g* (Millipore). Protein concentrations were determined by OD_{280}, correlated to Bradford and Micro BSA kit (Pierce) assayed values for TIM. The reference OD_{280} value of 35075 M^{-1} cm^{-1} was calculated with the ProtParam tool (*45*).

Enzymatic Assays. Triosephosphate isomerase activity for TbTIM and P168A was assayed at 25 °C as previously described (*29*). GAP was purified by use of Dowex 50. With GAP as substrate, the assay mixture contained NADH (0.3 mM), glycerol-phosphate dehydrogenase (GDH) (0.04 mg mL^{-1}), and GAP (0.1−6 mM) in 0.3 mL of buffer A. Residual TIM activity in the GDH sample was inactivated by incubation with BHAP, as previously described (*29*). TbTIM (4.5 ng) or P168A (92 ng) was used to initiate the reaction. With DHAP as substrate, the assay mixture contained NAD^+ (0.3 mM), potassium arsenate (5 mM), glyceraldehyde-3-phosphate dehydrogenase (0.17 mg mL^{-1}), and DHAP (0.3−40 mM). TbTIM (98 ng) or P168A (1700 ng) was used to initiate the reaction.

Initial rates were measured at each substrate concentration from the change in NADH absorbance at 340 nm with a Powerwave X microtiterplate reader (Bio-tek Instruments). Path length corrections were measured according to the manufacturer and confirmed with a NADH solution (0.05 mM) using a spectrophotometer and a 1 cm cuvette at 340 nm. The k_{cat} and K_m values were obtained after data fitting to the Michaelis−Menten equation using GraFit (Erithacus Software, Stains, U.K.). K_i values for arsenate and 2PG were determined assuming a competitive inhibition model (*29*). Protein concentrations were measured with a nanodrop photospectrometer (Nanodrop) at OD_{280} prior to the assay.

Thermal Stability. The CD spectra were recorded with a Jasco J-715 spectropolarimeter with a path length of 1 mm at 25 °C before and after the temperature-induced denaturation studies. A baseline spectrum of the buffer was subtracted from the sample spectra. Temperature denaturation studies were carried out by monitoring the ellipticity from 20 to 60 °C at 222 nm with a rate of 30 °C/h. Samples were kept at 60 °C for less than 1 min, after which the ellipticity was monitored from 60 to 20 °C. Protein solutions (0.4 mg mL^{-1}) were in 0.9 mM TEA and 1.2 mM NaCl, pH 7.5, containing also 0.05 mM DTT, 0.05 mM EDTA, and 0.05 mM sodium azide.

Crystallography. The initial crystallization experiments were done using the Factorial 1 screen, as previously described (*46*) at +22 °C with the hanging drop method. The drops were made by mixing 2 μL of protein solution and 2 μL of well solution. The unliganded P168A crystals were grown using 11 mg mL^{-1} protein solution in buffer C and 0.1 M TEA, pH 7.0, 27% PEG2000-MME, and 200 mM KSCN as well solution. The 2PG-P168A complex was crystallized with well solution: 0.1 M CHES, pH 9.5, 25% PEG1500, and 200 mM $MgSO_4$ and using 11.5 mg mL^{-1} protein solution in buffer C, containing 10 mM 2PG.

The 2.1 Å dataset of the unliganded P168A crystal was collected with a Nonius FR591 rotating anode X-ray generator, equipped with a Marresearch MAR345 image plate. The 1.15 Å dataset of the P168A-2PG crystal was collected at beamline BW7A, EMBL/DESY, Hamburg, Germany, using a Marresearch MAR CCD 165 mm detector. Before the crystals were flash frozen with a cold nitrogen stream at 100 K for data collection 2 μL of a 50% paraffin oil in silicone oil solution (v/v) was added on top of the drop to prevent the mounted crystal from drying out. The data were processed using the program XDS version December 2003 (*47*) with the interface XDSi version 1.2 (*48*). The data collection statistics are summarized in Table 1. Using programs F2MTZ and CAD from the CCP4 package (*49*) 5% of the observed structure factors were flagged and used for the free *R*-factor calculations. The structures were solved using molecular replacement with the program MOLREP version 7.3.01 (*50*) using 5TIM (*11*) as a search model and refined with REFMAC5 version 5.2.0005 (*51*). Weak NCS restraints were used in the REFAMC5 refinement protocol. The anisotropic motion of the subunits was described with the TLS parameters as implemented in REFMAC5 (*51*). Both the molecular replacement and refinement of structures were done using the CCP4 program suite version 5.0 with the interface version 1.3.2 (*49*). The final refinement of P168A in complex with 2PG was done using SHELXH version 97-2 (*52*), without using NCS restraints. The manual rebuilding was done using the program XFIT of the XTALVIEW package version 4.1 (*53*). Water molecules were added manually and by using

Table 1: Data Processing and Refinement Statistics

	P168A	P168A-2PG
Data Collection		
space group	*P*1	*P*212121
unit cell dimensions		
a, *b*, *c* (Å)	37.50, 43.72, 71.27	45.81, 97.32, 112.74
α, *β*, *γ* (deg)	80.5, 79.6, 64.7	90.0, 90.0, 90.0
resolution range (Å)[a]	25−2.1 (2.2−2.1)	25.0−1.15 (1.2−1.15)
R_{merge} (%)[a]	7.1 (13.3)	5.7 (34.5)
$I/\sigma I$[a]	13.8 (8.7)	25.1 (5.3)
completeness (%)[a]	94.5 (92.2)	92 (76.3)
redundancy[a]	2.7 (2.6)	6.8 (4.9)
no. of unique reflections	22102	164758
Wilson *B*-factor (Å^2)	17.7	11.6
Refinement		
resolution range (Å)	25.0−2.1	25−1.15
protein atoms	3808	3788
ligand atoms	0	23
water molecules	399	686
R (%)	14.9	14.2
R_{free} (%)	23.0	19.0
rmsd bond length (Å)	0.017	0.013
rmsd bond angle (deg)	1.6	
rmsd bond angle (DANG) (Å)		0.028
anisotropic displacement parameters		
DELU (Å^2)		0.005
SIMU (Å^2)		0.045
ISOR (Å^2)		0.081
rmsd *B* factors (Å^2)		
main chain	0.8	
side chain	1.8	
average *B* (Å^2)		
protein, main chain	7.4	8.1
protein, side chain	8.3	11.7
ligand		7.2
solvent	13.6	22.6
Ramachandran plot		
most favored region (%)	93	94
additionally allowed region (%)	7	6
NCS information		
rmsd of *β*-sheet Cα atoms of subunits A and B (Å)	0.1	0.1

[a] The numbers in parentheses refer to the highest resolution bin.

programs ARP/wARP version 6.1.1 (*54*), XTALVIEW package version 4.1 (*53*), and SHELXH version 97−2 (*52*). The quality of the structures was checked with PROCHECK (*55*). The final refinement statistics of both structures are summarized in Table 1.

Structure Analysis. For the structure comparisons the following structures were used: 5TIM (TbTIM, refined at 1.83 Å), 1YDV (plasmodium TIM, unliganded, 2.2 Å resolution), 1YPI (yeast TIM, unliganded, 1.9 Å resolution), 1N55 (leishmanial TIM, complexed with 2PG, refined at 0.83 Å), 1TPH (chicken TIM, complexed with the transition state analogue phosphoglycolohydroxamate, 1.8 Å resolution), and 1NEY (yeast TIM, complexed with DHAP, 1.2 Å resolution). In 5TIM, the A-subunit is unliganded (open) and the B-subunit is liganded ("almost closed") with a sulfate ion bound in the active site. In the atomic resolution structure 1N55 there is only one subunit per asymmetric unit; in case of double conformations of this entry only the main conformation has been used. The wild-type reference structures are 5TIM(A) and 1N55. The superpositions were done using the 36 Cα atoms of the *β*-sheet residues, being residues 7−11, 38−42, 61−64, 90−93, 122−127, 163−166, 207−210, and 230−233. The structures have been analyzed with O (*56*) and the ICM program version 3.4-2d (Molsoft L.L.C., La Jolla, CA); the pictures were made using ICM.

Table 2: Steady-State Kinetic Parameters for TbTIM and P168A

	TbTIM[a]	P168A[a]	units	TbTIM/P168A
k_{cat}(GAP)	3570 ± 420	60 ± 14	s^{-1}	59
K_m(GAP)	0.26 ± 0.04	0.16 ± 0.04	mM	1.6
k_{cat}/K_m(GAP)	13570 ± 2780	390 ± 130	s^{-1} mM^{-1}	35
k_{cat}(DHAP)	645 ± 110	19 ± 7	s^{-1}	34
K_m(DHAP)	0.9 ± 0.2	0.5 ± 0.3	mM	1.7
k_{cat}/K_m(DHAP)	730 ± 200	36 ± 26	s^{-1} mM^{-1}	20
K_i(2PG)	0.05	0.3 ± 0.1	mM	0.2
$K_i(HAsO_4^{2-})$	4.9 ± 0.1	5.8 ± 3.0	mM	0.8

[a] All values [except K_i(2-PG) of TbTIM] are the average of multiple, independent measurements. The values of TbTIM agree well with previously reported results (*66*).

RESULTS

Enzyme Kinetics. The steady-state kinetic parameters of the P168A variant were determined for both the forward and the reverse reactions. The kinetic constants are compared with the TbTIM data in Table 2. The turnover numbers (k_{cat}) of the P168A variant for both reactions are approximately 50 times lower than for TbTIM, whereas the K_m values are reduced by approximately 40%, indicating a higher affinity of P168A for both of its substrates. Interestingly, the K_i values for arsenate and 2PG show that P168A has a lower affinity for both of these inhibitors: for arsenate the affinity is slightly lower (by 20%) and for 2PG the affinity of the mutant is significantly (5 times) lower.

Thermal Stability. The CD melting curves, recorded at a wavelength of 222 nm (Figure 3), indicate that the thermal stabilities of unliganded TbTIM and P168A are the same. Analysis of the melting curves suggests a melting temperature of 51 °C, in agreement with previous experiments (*57*). For both proteins the heat-induced denaturation is irreversible, as suggested from refolding experiments when cooling the sample back to 20 °C after completion of the heat denaturation protocol (data not shown).

Structural Studies. High-resolution crystal structures have been determined for the unliganded and liganded P168A TIM variant at 2.1 and 1.15 Å, respectively. Each structure has a dimer in the asymmetric unit. There are no outliers in the Ramachandran plot. The conformation of all residues of the polypeptide chain is well-defined by the corresponding regions of the electron density map. The structure analysis

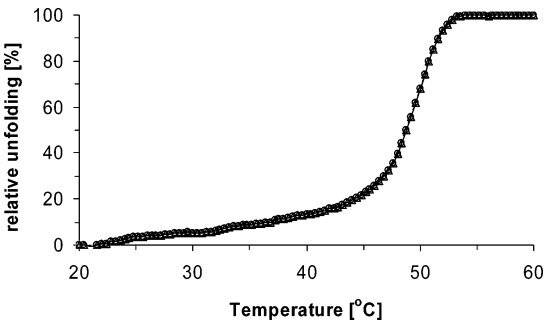

FIGURE 3: The CD melting (T_m) curves of TbTIM (△) and the P168A variant (○).

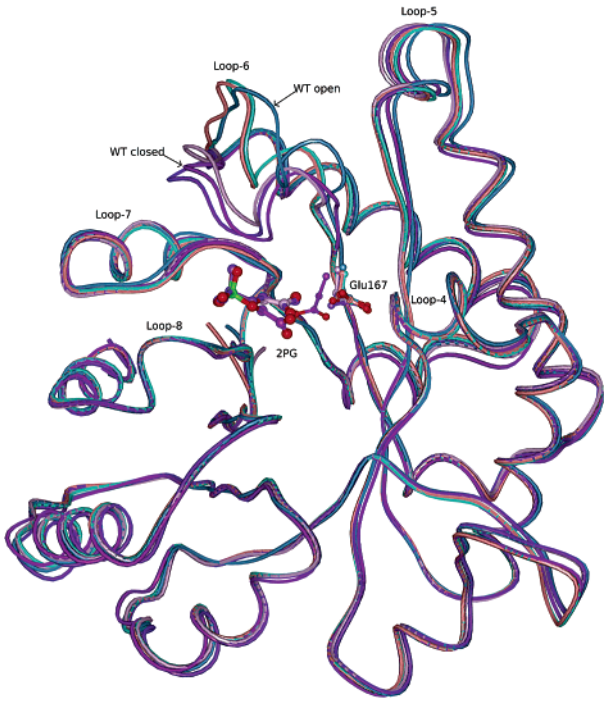

FIGURE 4: Superimposed Cα traces of wild-type TIM (liganded and unliganded) with P168A liganded (subunits A and B) and P168A unliganded (subunits A and B), highlighting the structural variability of loop 6 of P168A. The unliganded/open wild-type TIM structure is colored cyan (labeled as WT open), and the liganded/closed wild-type TIM structure is colored magenta (labeled as WT closed). Also included in ball-and-stick representation, using the same color code, are the transition state analogue 2PG and the side chain of the catalytic glutamate of each of the structures.

has been done with the A-subunit of each of the respective dimers; reference to the B-subunits is made whenever there are significant structural differences with respect to the A-subunit. The *B*-factor plots of the Cα atoms and the electron density maps show that loop 6 is well-defined in the liganded and unliganded P168A structures, except for the tip of the closed conformation of loop 6 of the B-subunit of the liganded structure, which has relatively high *B*-factors. This is in contrast with the wild-type structures, where it has been found that, characteristically in the closed liganded structures, loop 6 is well ordered and has low *B*-factors, whereas the unliganded, open conformation of loop 6 has higher *B*-factors (*19*). The electron density maps also show that the structure of the Glu167-Ala168 dipeptide is very well defined in each structure.

DISCUSSION

Comparison of the TbTIM and P168A Structures. In this mutagenesis experiment the three carbon atom side chain of Pro168 is changed into a one carbon atom side chain of the new residue, Ala168. The introduction of this smaller side chain has not decreased the stability in a measurable way (Figure 3). However, the lower catalytic efficiency of the P168A TIM variant confirms the importance of a proline at this position for the function of TIM. The structural changes due to the P168A mutation are visualized in Figures 4−6. As in wild-type TIM loop 6 can adopt an open and closed conformation in the P168A mutant.

A key feature of the closing of loop 6 is the movement of the side chain of Trp170. In the mutant structures this movement of the Trp170 side chain also occurs (Figure 5). However, the comparison of the Cα traces highlights the greater structural variability of loop 6 in particular for the liganded-closed mutant structures. From previous structural studies it is known that in the wild-type structures loop 6 adopts either a unique open or closed conformation (*19*, *25*). Apparently, the P168A mutation allows for greater structural variability of loop 6 in this variant. Small shifts occur also in loop 5, whereas there are no structural differences for loop 7. In the mutant, loop 7 (Figures 5 and 6) adopts either the open (unliganded) structure or the closed (liganded) structure, as in wild-type TIM (*30*).

Figures 5 and 6 show that in the mutant structures the main chain near residue 168 adopts a path slightly different from that of wild type. Given the high quality of the maps in these regions, these structural differences are significant. The structure of the Glu167-Ala168 dipeptide is identical for each of the two subunits of the same dimer and virtually the same when comparing the liganded and unliganded mutant structures (Figure 5). As in wild-type TIM, this dipeptide has low *B*-factors. In the comparison of the unliganded wild-type and mutant structures the largest differences (approximately 1.1 Å) are seen near the main chain of residue 168.

In the liganded structure of the P168A variant, the peptide nitrogen of Ala168 is hydrogen bonded to O(Gly211) of loop 7. In the unliganded structure this O(Gly211) is in a different position and thus not able to make such a hydrogen-bonding interaction. In wild-type TIM this hydrogen-bonding interaction is also not possible in either the liganded or the unliganded structure because of the covalent bond between N(Pro168) and the CD atom of its proline ring. The side chain of Pro168 points inward toward the bulk of the protein, away from the side chain of the catalytic glutamate (Figure 2), and the water structure near Glu167 of the wild-type TIM and P168A is the same.

Another characteristic feature of the wild-type open, unliganded structure is the hydrogen-bonding interaction between the main chain peptide oxygen of Glu167 with N(Val169) (Figure 7). This geometry has been referred to as a γ'-turn (*58*−*60*). The existence of such turns in several proteins, in particular near active sites, has been described (*60*). This turn is also referred to as $C7^{eq}$ because it concerns a seven-membered ring in which the β-carbon atom is equatorial to the ring. Its inverse structure is the γ-turn ($C7^{ax}$), which is also observed in protein structures; its preferred ϕ/ψ values are +75°/−60° (*58*). The preferred values of the γ'-turn are −75°/+60°, for the middle residue of the turn, which in this case is Pro168. In the wild-type open structure the ϕ/ψ values of Pro168 are −77°/82° (Table 3). In the wild-type closed structure the proline side chain is pushed away by the flipped peptide oxygen of Gly211 (Figure 2), and its ϕ/ψ values are −58°/133° (Table 3), and consequently the γ'-turn hydrogen bond is broken in this closed structure. The ϕ value of a proline can only adopt restricted values, because of its pyrrolidine side chain; a statistical analysis of many structures in the PDB has shown that the preferred range of the ϕ values of a proline is $-76° \pm 30°$ (*15*). The ψ values of prolines can adopt a wide range of values but are centered around three regions, being $\psi = 140°$, $\psi = 85°$, and $\psi = -30°$ (*58*). In the switch from unliganded to liganded the Pro168 ψ value changes from the second region

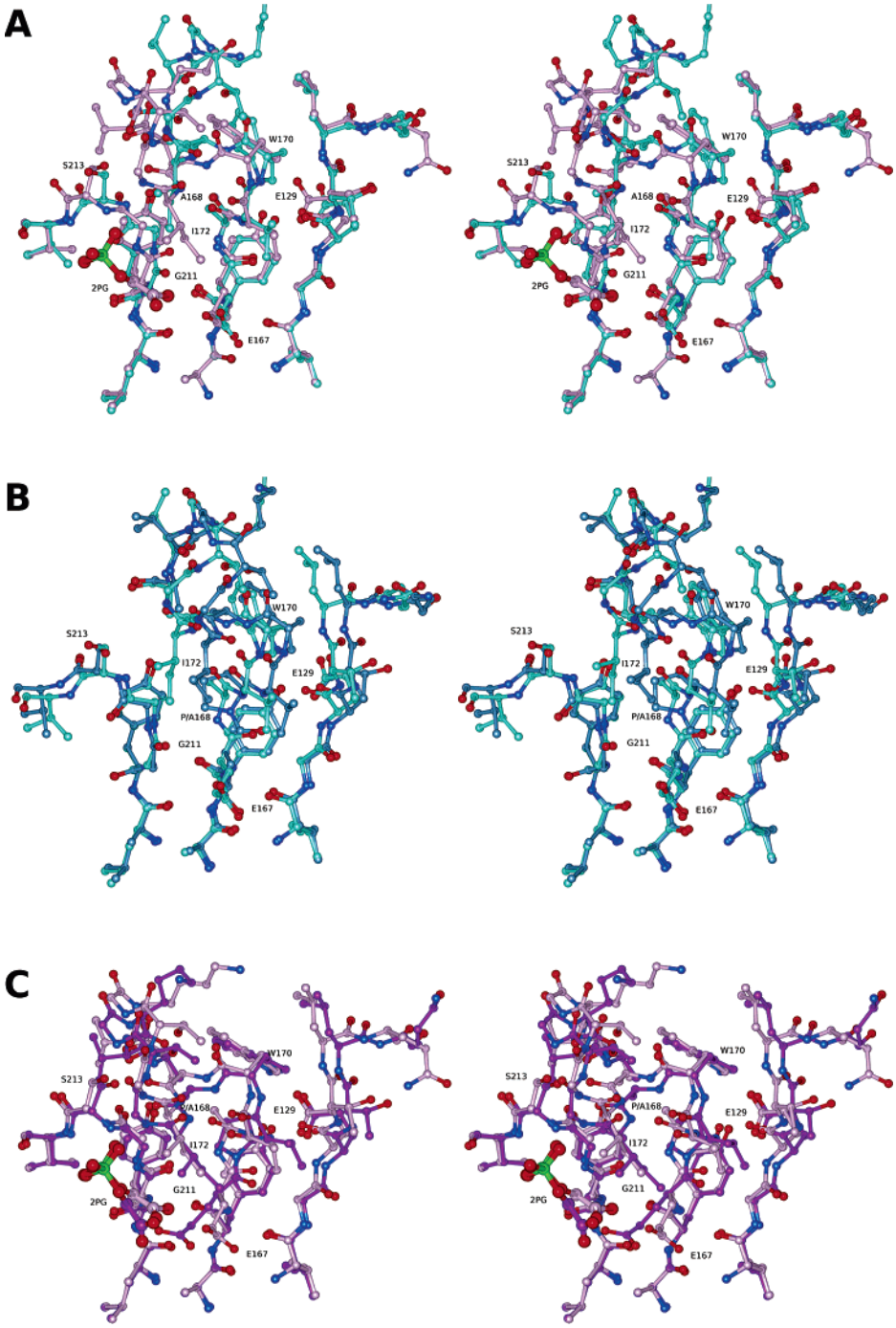

FIGURE 5: Structure comparison of loop 5 (residues 127−132), loop 6 (residues 165−178), and loop 7 (residues 209−214). In particular, the different conformations of the 167−168 dipeptide of wild type and P168A are emphasized. (A) Comparison of the liganded (gray) and unliganded (light blue) P168A structures. (B) Comparison of the unliganded structures of P168A (light blue) and wild-type TIM (cyan). (C) Comparison of the liganded structures of P168A (gray) and wild-type TIM (purple).

to the first region. Residues before a proline have been classified by MacArthur and Thornton (*15*) in a special group with unique conformational properties, avoiding ϕ/ψ values of the central β-region (near −120°, 135°) and populating a unique region (near −130°, 80°) (*14*, *58*). The ϕ/ψ values of Glu167 in wild type are −107°/112° and −128°/100° (Table 3) for the open and closed conformations, respectively, which both are in the allowed region of the Ramachandran plot for X-Pro residues.

In the P168A mutant, the hydrogen-bonding interaction of the γ'-turn of Ala168 is well preserved in the unliganded structure (as compared to wild type), and it remains intact when the tip of loop 6 closes. The ϕ/ψ values (approximately −80°/+80°) of Ala168 are very much the same in the liganded and unliganded structure (Table 3). As is shown in Figure 5, the Glu167-Ala168 region of the P168A variant does not move on ligand binding, whereas in all wild-type structures the main chain of Glu167 slightly adjusts when loop 6 closes (Figure 7, Table 3). It has been speculated previously (*11*, *17*) that the small adjustment of the main chain near Glu167 is an important structural tool to facilitate the movement of the side chain of Glu167 from the swung-

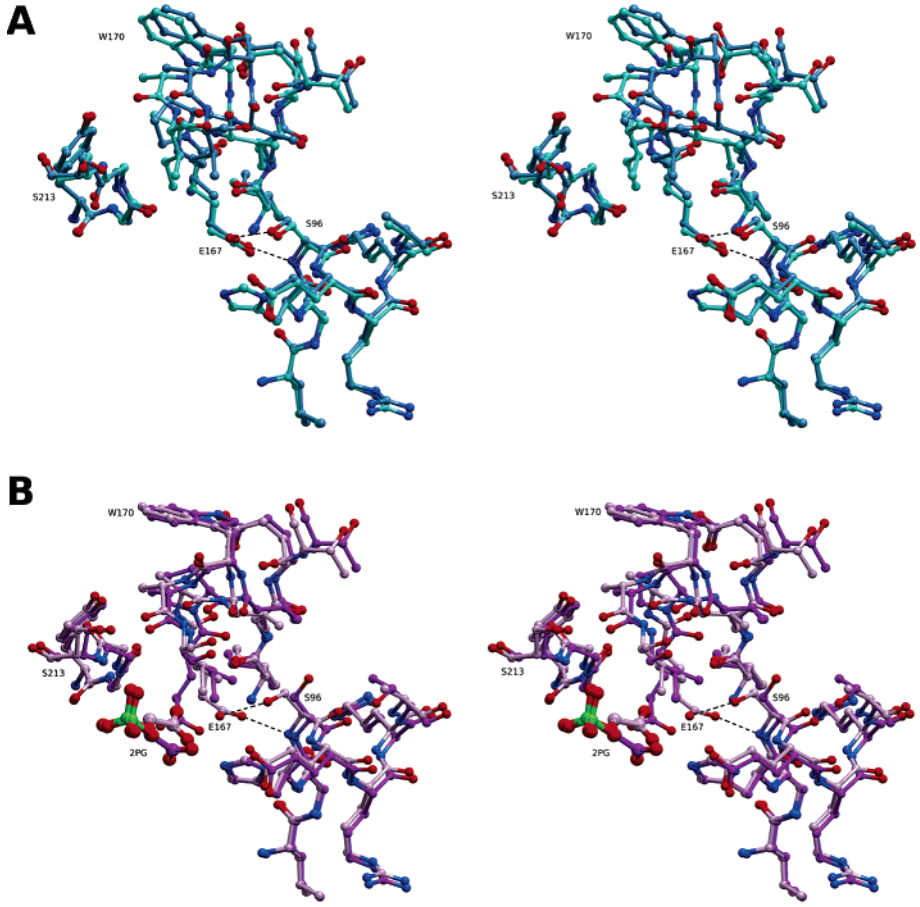

FIGURE 6: Structure comparison of loop 4 (residues 93−100), loop 5 (residues 127−130), loop 6 (residues 166−170), and loop 7 (residues 210−213). The different interactions of the side chain of Glu167 in wild type and the P168A variant are also visualized. (A) Comparison of the unliganded P168A (light blue) and wild-type TIM structures (cyan). (B) Comparison of the liganded P168A (gray) and wild-type TIM structures (purple). The dotted lines indicate the hydrogen-bonding interactions between Glu167 and Ser96.

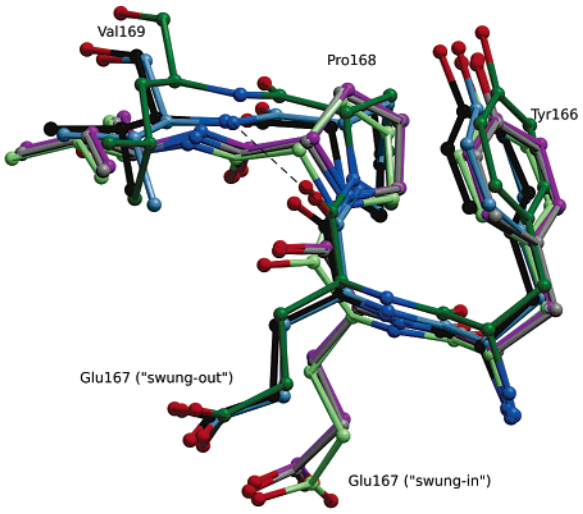

FIGURE 7: Structure analysis of the Tyr166-Glu167-Pro168-Val169 region of unliganded TIM [trypanosomal (light blue), plasmodium (dark green), and yeast (black)] and liganded TIM [chicken (light green), yeast (gray), and leishmania (magenta)]. The γ'-turn hydrogen bond between O(Glu167) and N(Val169) in the unliganded structures is highlighted by a dotted line; in these structures the Glu167 side chain is in the swung-out conformation. The labeling refers to the trypanosomal TIM structures.

out to the swung-in position. This proposal was originally put forward from the observation that in an almost closed structure with a sulfate ion bound in the binding pocket (subunit B of 5TIM) the small main chain rearrangement

Table 3: Main Chain and Side Chain Geometry of the Region Tyr166-Glu167-Pro168

		ϕ	ψ	χ_1
Tyr166	5TIM-A (unliganded/open)	−91	115	178
	1N55 (liganded/closed)	−87	114	173
	5TIM-B (liganded/almost closed)	−100	104	171
	P168A-A (unliganded)	−88	100	173
	P168A-B (unliganded)	−92	98	172
	P168A-A (liganded)	−88	116	166
	P168A-B (liganded)	−87	115	165
Glu167	5TIM-A (unliganded/open)	−107	112	−57
	1N55 (liganded/closed)	−128	100	−53
	5TIM-B (liganded/almost closed)	−122	99	69
	P168A-A (unliganded)	−81	110	−71
	P168A-B (unliganded)	−79	110	−75
	P168A-A (liganded)	−102	125	−59
	P168A-B (liganded)	−103	120	−63
P168A	5TIM-A (unliganded/open)	−76	82	40
	1N55 (liganded/closed)	−58	134	3
	5TIM-B (liganded/almost closed)	−57	107	2
	P168A-A (unliganded)	−83	70	
	P168A-B (unliganded)	−86	69	
	P168A-A (liganded)	−80	94	
	P168A-B (liganded)	−75	94	

near Glu167 has occurred but its side chain is still in the swung-out position. In this structure of loop 6 (closed, but Glu167 is swung-out) χ_1 of the Glu167 side chain has adopted the unfavorable value of +60° (Table 3), whereas in the open, swung-out position $\chi_1 = -60°$ (Table 3). In at least two other liganded structures, being the complexes with the bulky substrate analogues 2-phosphoglycerate (*61*) and

3-phosphoglycerate (*62*), loop 6 is also closed with Glu167 still in the swung-out conformation with χ_1 near $+50^\circ$. In this swung-out conformation the Glu167 side chain oxygen atoms are hydrogen bonded to N(Ser96) and OG(Ser96), respectively, as in the wild-type TIM open conformation (Figures 2 and 6). In active sites with tight binding substrate analogues, such as 2PG (Figure 7), the side chain conformational change to swung-in causes the χ_1 to again adopt the favorable value of -60° (Table 3), and the Glu167 side chain points to the ligand (the swung-in conformation). Combining the available structural data of the wild-type active site geometry suggests that the small Glu167 main chain rearrangement (as seen in wild-type TIM on ligand binding) facilitates the conformational change of the Glu167 side chain from the inactive swung-out position to the active swung-in position. In P168A the Glu167-Pro168 region does not rearrange on ligand binding (Figure 5), and the side chain of Glu167 remains in the swung-out position and remains hydrogen bonded to Ser96 (Figure 6). As a consequence, the Ser96 side chain does not rotate away from its open conformation to its closed conformation, which also prevents the fully closed wild-type loop 6 conformation because of a potential clash (2.3 Å) between the CD1(Ile172) (closed) and OG(Ser96) (open) (Figure 6).

The properties of the proline side chain of Pro168 are apparently in a subtle but crucial way needed to couple the ligand binding and loop 6 closure to the small main chain rearrangement of Glu167, which then facilitates the activation of this catalytic side chain. Two structural properties of the proline ring of Pro168 of the wild type are important in this respect: (i) the absence of a hydrogen bond between N(Pro168) and O(Gly211) (this hydrogen bond is present in P168A, liganded, and stabilizes the open conformation of the Glu167-Ala168 region) and (ii) the proline ring itself, in particular its CD atom. This atom is pushed away in wild-type TIM by O(Gly211) after the peptide rotation, and thereby Pro168 adopts its liganded, closed conformation. There is no evidence that the proline is especially important for possible unique dynamical properties of the wild-type active site, because both in wild type and in mutant the 167−168 dipeptide has low *B*-factors.

Mode of Binding of 2-Phosphoglycolate. The interactions of the phosphate moiety of the ligand with loop 7 and loop 8 atoms are the same in the wild-type and mutant structures; however, the catalytic end of the transition state analogue is bound in a different way. The strong hydrogen bond between the carboxylate oxygens of Glu167 and 2PG, present in the wild-type complex (*12*), is absent in the mutant complex. Instead, this part of the ligand is bound further "up" (Figure 8), which is possible only because Glu167 is in the swung-out conformation. This up mode of binding prevents Ile172 (as well as the tip of loop 6) to adopt the fully closed conformation. Consequently, the hydrogen bonding of the tip of loop 6 with the phosphate moiety is not as optimal as seen in the wild-type complex. This loose interaction correlates with the relatively high *B*-factor of the tip of loop 6 in one of the subunits of the complex of the P168A mutant. Also, the lower affinity of 2PG for the mutant enzyme can be understood from the structural differences between the wild-type complex and the mutant complex.

The high affinity of the transition state analogue 2PG for the wild-type TIM active site reflects the close proximity of

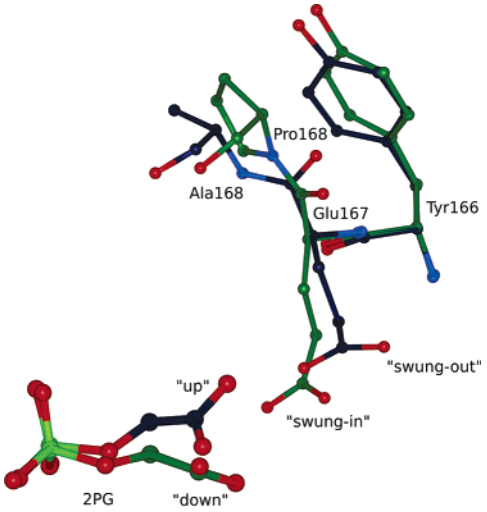

FIGURE 8: Schematic view of the mode of binding of 2PG in P168A (carbon atoms are colored cyan) and wild-type TIM (carbon atoms are colored green). In the latter complex the side chain of Glu167 adopts the active swung-in conformation and 2PG is bound in the down mode of binding. In the P168A complex the Glu167 side chain remains in the swung-out state and the 2PG mode of binding is different (up mode of binding).

the catalytic Glu167 side chain to the C1 and C2 substrate atoms during the formation of the transition state (*17*). In the liganded P168A structure the Glu167 side chain is seen in the "swung-out" conformation, and there are no hydrogen bonds between 2PG and Glu167. This nonactive swung-out conformation of the catalytic glutamate in the structure of the P168A-2PG complex correlates well with the lower turnover numbers of the P168A variant.

The Closing Mechanism of Loop 7 and Loop 6. Elegant NMR studies of the loop 6 dynamics by McDermott (*20*, *21*) have highlighted that loop 6 samples the closed conformation in the unliganded state as well as the open conformation in the liganded state. T-jump experiments on the sequential events associated with ligand binding by Callender and colleagues (*22*) have shown that in this binding process first an initial encounter complex (presumably the liganded, but open structure) is formed, followed by a structural change resulting in the closed structure. Indeed, crystal structures of the open form of wtTIM, complexed to a ligand, have been observed, for example, for plasmodium TIM (*26*, *63*). In these structures the ligand interacts with loop 7 (and not with loop 6). This suggests that the first effect of ligand binding to wild-type TIM is the conformational switch of loop 7, resulting in a better interaction between the phosphate moiety of the ligand and loop 7. Subsequently, the conformational change of loop 6 follows. This conformational change of loop 6 is facilitated, or even triggered, by the movement of O(Gly211) in loop 7, as it clashes with CD(Pro168) (Figure 2). This clash occurs if the Pro168 side chain would not move (Figure 2) after O(Gly211) has rotated to its new position. In the P168A variant this clash does not occur, because the main chain conformation at residue 168 is different in the P168A variant as compared to wild type (Figures 5 and 6). Consequently, ligand binding, followed by the conformational change of loop 7, does not induce structural rearrangements of the Glu167-Ala168 region (Figures 5 and 8) in the P168A variant. The closed conformation of loop 6 is nevertheless

observed in the P168A TIM variant; it is stabilized by hydrogen bonding with the phosphate moiety of the ligand and with the loop 7 side chains Tyr210 and Ser213, as in wtTIM. In the wild-type TIM (but not in the mutant) the Glu167 side chain adopts the swung-in conformation when loop 6 is closed, favoring the "down" mode of binding of the transition state analogue (Figure 8).

The sequential timing of the conformational changes facilitated by ligand binding suggests that the loop 7 conformational switch is the key step, whereas the structural change of loop 6 is a consequence of this: once loop 7 has adopted its closed conformation, then the most stable conformation of loop 6 is its closed conformation. In line with this hypothesis is the observation that the mode of binding of the phosphate moiety of 2PG is the same in the wild type and mutant. Also, the affinity for arsenate is similar in wild type and mutant, whereas the affinity for 2PG is lower in the mutant. The latter observation can be understood from the changed structural properties of Glu167 in the mutant, which does affect the mode of binding of the carboxylic end of 2PG but not the mode of binding of the phosphate moiety. Similar observations were made previously with another loop 6 variant in which the tip of the loop was deleted (*64*). For this variant the affinity for the transition state analogue phosphoglycolohydroxamate was also much lower, but the affinity for arsenate was very similar as in wild type. In this respect it is also interesting to point out that the loop 7 conformational switch involves a high-energy barrier, being the rotation of the peptide planes of the YGGS peptide. The ϕ/ψ values of Tyr210, Gly211, Gly212, and Ser213 change from respectively −94°/124°, −111°/18°, −86°/−160°, and −83°/118° (open) to −104°/142°, −144°/160°, 123°/95°, and 65°/28° (closed). In particular, the conformational changes of Gly212 and Ser213 are known to be associated with a high-energy barrier (*58*, *65*). Future computational studies will be needed to confirm that the rate-limiting step of the closure of the TIM active site is not the loop 6 conformational change but instead the loop 7 conformational switch.

Concluding Remarks. Summarizing, the combined results of these kinetic and structural studies rationalize the importance of Pro168 for the proper functioning of TIM. The structural studies show that in the P168A mutant the properties of loop 7 have not changed, whereas the structural properties of the Glu167-Ala168 dipeptide of loop 6 are different from those of wild type. In wild-type TIM the rigidity of the proline ring, including the potential clash of the CD atom of Pro168 with O(Gly211) of loop 7, favors loop 6 closure, once substrate binding has facilitated the formation of the closed conformation of loop 7. Additionally, stabilizing hydrogen-bonding interactions freeze the active site in a catalytically incompetent state in the P168A variant. The different hydrogen-bonding properties of the proline of wild-type TIM facilitate the concerted conformational change of loop 7 and the Glu167-Pro168 region of loop 6. The conformational change of this Glu167-Pro168 dipeptide is required to generate the catalytically competent Glu167 swung-in conformation of wild-type TIM.

ACKNOWLEDGMENT

We have much appreciated the help from the staff at the beamline BW7A (EMBL/DESY in Hamburg) for collecting the data of the liganded P168A structure. The skillful technical support from Ville Ratas has been invaluable in this work.

REFERENCES

1. Wolfenden, R. (1969) Transition state analogues for enzyme catalysis, *Nature 223*, 704−705.
2. Fersht, A. (1999) *Structure and Mechanism in Protein Science. A Guide to Enzyme Catalysis and Protein Folding*, W. H. Freeman, New York.
3. Herzberg, O., and Moult, J. (1991) Analysis of the steric strain in the polypeptide backbone of protein molecules, *Proteins 11*, 223−229.
4. Meiering, E. M., Serrano, L., and Fersht, A. R. (1992) Effect of active site residues in barnase on activity and stability, *J. Mol. Biol. 225*, 585−589.
5. Shoichet, B. K., Baase, W. A., Kuroki, R., and Matthews, B. W. (1995) A relationship between protein stability and protein function, *Proc. Natl. Acad. Sci. U.S.A. 92*, 452−456.
6. Rose, I. A. (1962) Mechanism of C−H bond cleavage in aldolase and isomerase reactions, *Brookhaven Symp. Biol. 15*, 293−309.
7. Knowles, J. R. (1991) Enzyme catalysis: not different, just better, *Nature 350*, 121−124.
8. Joseph, D., Petsko, G. A., and Karplus, M. (1990) Anatomy of a conformational change: hinged "lid" motion of the triosephosphate isomerase loop, *Science 249*, 1425−1428.
9. Sampson, N. S., and Knowles, J. R. (1992) Segmental movement: definition of the structural requirements for loop closure in catalysis by triosephosphate isomerase, *Biochemistry 31*, 8482−8487.
10. Lolis, E., and Petsko, G. A. (1990) Crystallographic analysis of the complex between triosephosphate isomerase and 2-phosphoglycolate at 2.5-Å resolution: implications for catalysis, *Biochemistry 29*, 6619−6625.
11. Wierenga, R. K., Noble, M. E., Vriend, G., Nauche, S., and Hol, W. G. (1991) Refined 1.83 Å structure of trypanosomal triosephosphate isomerase crystallized in the presence of 2.4 M-ammonium sulphate. A comparison with the structure of the trypanosomal triosephosphate isomerase-glycerol-3-phosphate complex, *J. Mol. Biol. 220*, 995−1015.
12. Kursula, I., and Wierenga, R. K. (2003) Crystal structure of triosephosphate isomerase complexed with 2-phosphoglycolate at 0.83-Å resolution, *J. Biol. Chem. 278*, 9544−9551.
13. Vitagliano, L., Berisio, R., Mastrangelo, A., Mazzarella, L., and Zagari, A. (2001) Preferred proline puckerings in cis and trans peptide groups: implications for collagen stability, *Protein Sci. 10*, 2627−2632.
14. Karplus, P. A. (1996) Experimentally observed conformation-dependent geometry and hidden strain in proteins, *Protein Sci. 5*, 1406−1420.
15. MacArthur, M. W., and Thornton, J. M. (1991) Influence of proline residues on protein conformation, *J. Mol. Biol. 218*, 397−412.
16. Donnini S, Groenhof, G., Wierenga, R. K., and Juffer, A. (2006) The planar conformation of a strained proline ring: a QM/MM study, *Proteins: Struct., Funct., Bioinf. 64* , 700−710.
17. Kursula, I., Salin, M., Sun, J., Norledge, B. V., Haapalainen, A. M., Sampson, N. S., and Wierenga, R. K. (2004) Understanding protein lids: structural analysis of active hinge mutants in triosephosphate isomerase, *Protein Eng., Des. Sel. 17*, 375−382.
18. Xiang, J., Sun, J., and Sampson, N. S. (2001) The importance of hinge sequence for loop function and catalytic activity in the reaction catalyzed by triosephosphate isomerase, *J. Mol. Biol. 307*, 1103−1112.
19. Kishan, K. V., Zeelen, J. P., Noble, M. E., Borchert, T. V., and Wierenga, R. K. (1994) Comparison of the structures and the crystal contacts of trypanosomal triosephosphate isomerase in four different crystal forms, *Protein Sci. 3*, 779−787.
20. Rozovsky, S., and McDermott, A. E. (2001) The time scale of the catalytic loop motion in triosephosphate isomerase, *J. Mol. Biol. 310*, 259−270.
21. Rozovsky, S., Jogl, G., Tong, L., and McDermott, A. E. (2001) Solution-state NMR investigations of triosephosphate isomerase active site loop motion: ligand release in relation to active site loop dynamics, *J. Mol. Biol. 310*, 271−280.
22. Desamero, R., Rozovsky, S., Zhadin, N., McDermott, A., and Callender, R. (2003) Active site loop motion in triosephosphate

isomerase: T-jump relaxation spectroscopy of thermal activation, *Biochemistry 42*, 2941−2951.
23. Cui, Q., and Karplus, M. (2003) Catalysis and specificity in enzymes: a study of triosephosphate isomerase and comparison with methyl glyoxal synthase, *Adv. Protein Chem. 66*, 315−372.
24. Guallar, V., Jacobson, M., McDermott, A., and Friesner, R. A. (2004) Computational modeling of the catalytic reaction in triosephosphate isomerase, *J. Mol. Biol. 337*, 227−239.
25. Aparicio, R., Ferreira, S. T., and Polikarpov, I. (2003) Closed conformation of the active site loop of rabbit muscle triosephosphate isomerase in the absence of substrate: evidence of conformational heterogeneity, *J. Mol. Biol. 334*, 1023−1041.
26. Parthasarathy, S., Balaram, H., Balaram, P., and Murthy, M. R. (2002) Structures of *Plasmodium falciparum* triosephosphate isomerase complexed to substrate analogues: observation of the catalytic loop in the open conformation in the ligand-bound state, *Acta Crystallogr., Sect. D: Biol. Crystallogr. 58*, 1992−2000.
27. Wierenga, R. K., Noble, M. E., Postma, J. P., Groendijk, H., Kalk, K. H., Hol, W. G., and Opperdoes, F. R. (1991) The crystal structure of the "open" and the "closed" conformation of the flexible loop of trypanosomal triosephosphate isomerase, *Proteins 10*, 33−49.
28. Xiang, J., Jung, J. Y., and Sampson, N. S. (2004) Entropy effects on protein hinges: the reaction catalyzed by triosephosphate isomerase, *Biochemistry 43*, 11436−11445.
29. Sun, J., and Sampson, N. S. (1999) Understanding protein lids: kinetic analysis of active hinge mutants in triosephosphate isomerase, *Biochemistry 38*, 11474−11481.
30. Noble, M. E., Zeelen, J. P., and Wierenga, R. K. (1993) Structures of the "open" and "closed" state of trypanosomal triosephosphate isomerase, as observed in a new crystal form: implications for the reaction mechanism, *Proteins 16*, 311−326.
31. Klaholz, B., and Moras, D. (2002) C−H·O hydrogen bonds in the nuclear receptor RARgamma−a potential tool for drug selectivity, *Structure 10*, 1197−1204.
32. Derewenda, Z. S., Lee, L., and Derewenda, U. (1995) The occurrence of C−H·O hydrogen bonds in proteins, *J. Mol. Biol. 252*, 248−262.
33. Jogl, G., Rozovsky, S., McDermott, A. E., and Tong, L. (2003) Optimal alignment for enzymatic proton transfer: structure of the Michaelis complex of triosephosphate isomerase at 1.2-Å resolution, *Proc. Natl. Acad. Sci. U.S.A. 100*, 50−55.
34. O'Donoghue, A. C., Amyes, T. L., and Richard, J. P. (2005) Hydron transfer catalyzed by triosephosphate isomerase. Products of isomerization of (*R*)-glyceraldehyde 3-phosphate in D_2O, *Biochemistry 44*, 2610−2621.
35. O'Donoghue, A. C., Amyes, T. L., and Richard, J. P. (2005) Hydron transfer catalyzed by triosephosphate isomerase. Products of isomerization of dihydroxyacetone phosphate in D_2O, *Biochemistry 44*, 2622−2631.
36. Zhang, Z., Komives, E. A., Sugio, S., Blacklow, S. C., Narayana, N., Xuong, N. H., Stock, A. M., Petsko, G. A., and Ringe, D. (1999) The role of water in the catalytic efficiency of triosephosphate isomerase, *Biochemistry 38*, 4389−4397.
37. Albery, W. J., and Knowles, J. R. (1976) Free-energy profile of the reaction catalyzed by triosephosphate isomerase, *Biochemistry 15*, 5627−5631.
38. Nickbarg, E. B., and Knowles, J. R. (1988) Triosephosphate isomerase: energetics of the reaction catalyzed by the yeast enzyme expressed in *Escherichia coli*, *Biochemistry 27*, 5939−5947.
39. Nam, G. H., Cha, S. S., Yun, Y. S., Oh, Y. H., Hong, B. H., Lee, H. S., and Choi, K. Y. (2003) The conserved cis-Pro39 residue plays a crucial role in the proper positioning of the catalytic base Asp38 in ketosteroid isomerase from *Comamonas testosteroni*, *Biochem. J. 375*, 297−305.
40. Mallis, R. J., Brazin, K. N., Fulton, D. B., and Andreotti, A. H. (2002) Structural characterization of a proline-driven conformational switch within the Itk SH2 domain, *Nat. Struct. Biol. 9*, 900−905.
41. Palfey, B. A., Basu, R., Frederick, K. K., Entsch, B., and Ballou, D. P. (2002) Role of protein flexibility in the catalytic cycle of *p*-hydroxybenzoate hydroxylase elucidated by the Pro293Ser mutant, *Biochemistry 41*, 8438−8446.
42. de Boer, T. J., and Backer, H. J. (1963) Generation of diazomethane, *Organic Syntheses*, Collect. Vol. 4, pp 250−253, Wiley, New York.
43. Husain, S. S., and Lowe, G. (1968) Evidence for histidine in the active site of papain, *Biochem. J. 108*, 855−859.
44. De la Mare, S., Coulson, A. F., Knowles, J. R., Priddle, J. D., and Offord, R. E. (1972) Active-site labelling of triose phosphate isomerase. The reaction of bromohydroxyacetone phosphate with a unique glutamic acid residue and the migration of the label to tyrosine, *Biochem. J. 129*, 321−331.
45. Gasteiger, E., Gattiker, A., Hoogland, C., Ivanyi, I., Appel, R. D., and Bairoch, A. (2003) ExPASy: The proteomics server for in-depth protein knowledge and analysis, *Nucleic Acids Res. 31*, 3784−3788.
46. Zeelen, J. P., Hiltunen, J. K., Ceska, T. A., and Wierenga, R. K. (1994) Crystallization experiments with 2-enoyl-CoA hydratase, using an automated "fast-screening" crystallization protocol, *Acta Crystallogr., Sect. D: Biol. Crystallogr. 50*, 443−447.
47. Kabsch, W. (1993) Automatic processing of rotation diffraction data from crystals of initially unknown symmetry and cell constants, *J. Appl. Crystallogr. 26*, 795−800.
48. Kursula, P. (2004) XDSi: a graphical interface for the data processing program XDS, *J. Appl. Crystallogr. 37*, 347−348.
49. Collaborative Computational Project Number 4 (1994) The CCP4 suite: programs for protein crystallography, *Acta Crystallogr., Sect. D: Biol. Crystallogr. 50*, 760−763.
50. Vagin, A., and Teplyakov, A. (1997) MOLREP: an automated program for molecular replacement, *J. Appl. Crystallogr. 30*, 1022−1025.
51. Murshudov, G. N., Vagin, A. A., and Dodson, E. J. (1997) Refinement of macromolecular structures by the maximum-likelihood method, *Acta Crystallogr., Sect. D: Biol. Crystallogr. 53*, 240−255.
52. Sheldrick, G. M., and Schneider, T. R. (1997) SHELXL: High-resolution refinement, in *Methods in Enzymology and Macromolecular Crystallography* (Charles, W. C., Jr., Ed.) Part B, Vol. 277, pp 319−343, Academic Press, New York.
53. McRee, D. E. (1992) A visual protein crystallographic software system for X11/Xview, *J. Mol. Graphics 10*, 44−46.
54. Lamzin, V. S., and Wilson, K. S. (1993) Automated refinement of protein models, *Acta Crystallogr., Sect. D: Biol. Crystallogr. 49*, 129−147.
55. Laskowski, R. A., MacArthur, M. W., Moss, D. S., and Thornton, J. M. (1993) PROCHECK: A program to check the stereochemical quality of protein structures, *J. Appl. Crystallogr. 26*, 283−291.
56. Jones, T. A., Zou, J. Y., Cowan, S. W., and Kjeldgaard (1991) Improved methods for building protein models in electron density maps and the location of errors in these models, *Acta Crystallogr. A 47* (Part 2), 110−119.
57. Schliebs, W., Thanki, N., Eritja, R., and Wierenga, R. (1996) Active site properties of monomeric triosephosphate isomerase (monoTIM) as deduced from mutational and structural studies, *Protein Sci. 5*, 229−239.
58. Lovell, S. C., Davis, I. W., Arendall, W. B., III, de Bakker, P. I., Word, J. M., Prisant, M. G., Richardson, J. S., and Richardson, D. C. (2003) Structure validation by Calpha geometry: phi, psi and Cbeta deviation, *Proteins 50*, 437−450.
59. Rose, G. D., Gierasch, L. M., and Smith, J. A. (1985) Turns in peptides and proteins, *Adv. Protein Chem. 37*, 1−109.
60. Milner-White, E. J. (1990) Situations of gamma-turns in proteins, their relation to alpha-helices, beta-sheets and ligand binding sites, *J. Mol. Biol. 216*, 386−397.
61. Noble, M. E., Verlinde, C. L., Groendijk, H., Kalk, K. H., Wierenga, R. K., and Hol, W. G. (1991) Crystallographic and molecular modeling studies on trypanosomal triosephosphate isomerase: a critical assessment of the predicted and observed structures of the complex with 2-phosphoglycerate, *J. Med. Chem. 34*, 2709−2718.
62. Noble, M. E., Wierenga, R. K., Lambeir, A. M., Opperdoes, F. R., Thunnissen, A. M., Kalk, K. H., Groendijk, H., and Hol, W. G. (1991) The adaptability of the active site of trypanosomal triosephosphate isomerase as observed in the crystal structures of three different complexes, *Proteins 10*, 50−69.
63. Parthasarathy, S., Ravindra, G., Balaram, H., Balaram, P., and Murthy, M. R. (2002) Structure of the *Plasmodium falciparum* triosephosphate isomerase-phosphoglycolate complex in two crystal forms: characterization of catalytic loop open and closed conformations in the ligand-bound state, *Biochemistry 41*, 13178−13188.
64. Pompliano, D. L., Peyman, A., and Knowles, J. R. (1990) Stabilization of a reaction intermediate as a catalytic device: definition of the functional role of the flexible loop in triosephosphate isomerase, *Biochemistry 29*, 3186−3194.

65. Hu, H., Elstner, M., and Hermans, J. (2003) Comparison of a QM/MM force field and molecular mechanics force fields in simulations of alanine and glycine "dipeptides" (Ace-Ala-Nme and Ace-Gly-Nme) in water in relation to the problem of modeling the unfolded peptide backbone in solution, *Proteins 50*, 451−463.

66. Lambeir, A. M., Opperdoes, F. R., and Wierenga, R. K. (1987) Kinetic properties of triose-phosphate isomerase from *Trypanosoma brucei brucei*. A comparison with the rabbit muscle and yeast enzymes, *Eur. J. Biochem. 168*, 69−74.

BI061683J